Maize *sugary enhancer1* (*se1*) is a gene affecting endosperm starch metabolism

Xia Zhang[a,b,1], Karl J. Haro von Mogel[a,1], Vai S. Lor[a,1], Candice N. Hirsch[c], Brian De Vries[a], Heidi F. Kaeppler[a], William F. Tracy[a], and Shawn M. Kaeppler[a,d,2]

[a]Department of Agronomy, University of Wisconsin-Madison, Madison, WI 53706; [b]Biotechnology Research Institute, Chinese Academy of Agricultural Sciences, 100081 Beijing, China; [c]Department of Agronomy and Plant Genetics, University of Minnesota, Saint Paul, MN 55108; and [d]Wisconsin Crop Innovation Center, University of Wisconsin-Madison, Madison, WI 53562

Edited by Brian A. Larkins, University of Nebraska, Lincoln, NE, and approved August 28, 2019 (received for review March 4, 2019)

***sugary enhancer1* (*se1*) is a naturally occurring mutant allele involved in starch metabolism in maize endosperm. It is a recessive modifier of *sugary1* (*su1*) and commercially important in modern sweet corn breeding, but its molecular identity and mode of action remain unknown. Here, we developed a pair of near-isogenic lines, W822Gse (*su1-ref/su1-ref se1/se1*) and W822GSe (*su1-ref/su1-ref Se1/Se1*), that Mendelize the *se1* phenotype in an *su1-ref* background. W822Gse kernels have lower starch and higher water soluble polysaccharide and sugars than W822GSe kernels. Using high-resolution genetic mapping, we found that wild-type *Se1* is a gene Zm00001d007657 on chromosome 2 and a deletion of this gene causes the *se1* phenotype. Comparative metabolic profiling of seed tissue between these 2 isolines revealed the remarkable difference in carbohydrate metabolism, with sucrose and maltose highly accumulated in the mutant. *Se1* is predominantly expressed in the endosperm, with low expression in leaf and root tissues. Differential expression analysis identified genes enriched in both starch biosynthesis and degradation processes, indicating a pleiotropic regulatory effect of *se1*. Repressed expression of *Se1 and Su1* in RNA interference-mediated transgenic maize validates that deletion of the gene identified as *Se1* is a true causal gene responsible for the *se1* phenotype. The findings contribute to our understanding of starch metabolism in cereal crops.**

maize | *sugary1* | *sugary enhancer1* | starch metabolism

Starch accumulated in cereal grains is the carbohydrate energy reserve used for human and animal nutrition and a major source of feedstock for numerous nonfood industrial uses. Starch also serves as the principal harvested component of our staple crop plants and, as such, has a major influence on crop yields and end-use quality (1). Therefore, a thorough understanding of the mechanistic basis of starch metabolism and regulation is critically important for meeting the future needs of both agricultural and industrial applications.

Starch typically consists of 2 glucose polymers, amylose and amylopectin. Amylose is predominantly a linear polymer composed of α-(1→4)–linked glucose units while amylopectin, comprising ∼75% of the starch, is a highly branched glucan with α-(1→6)–linked glucosidic bonds that connect linear chains. Starch biosynthesis in the cereal endosperm involves the coordinated activities of a suite of starch metabolic enzymes, including adenosine 5′ diphosphate-glucose (ADP-Glc) pyrophosphorylase (AGPase), starch synthases (SSs), starch branching enzymes (BEs), and starch debranching enzymes (DBEs) (2, 3). In maize (*Zea mays* L.), major advances in the distinct roles of these essential starch enzymes have been accomplished through research on various starch mutants, which identified key genes involved in the starch biosynthesis pathway, including starch-branching enzyme *amylose extender1* (*Ae1*) (4, 5), *brittle2* (*Bt2*) (6), Suc synthase *shrunken1* (*Sh1*) (7), large subunit of AGPase *shrunken2* (*Sh2*) (8), isoamylase-type DBE *sugary1* (*Su1*) (9), and granule-bound starch synthase *waxy1* (*Wx1*) (10). However, there are still major gaps in our knowledge of the biochemistry and pathways of starch synthesis and interactions among biosynthetic enzymes, as well as modifying factors that regulate enzyme activity. The pathway of starch degradation is not as well defined as that of starch biosynthesis. Knowledge about the process of starch degradation mainly arose from extensive studies in germinating cereal seeds and *Arabidopsis* leaves (11). Multiple forms of several starch-degrading enzymes have been found in cereal endosperm, including endo- and exo-amylases (α- and β-amylases, respectively), glucosidases, and debranching enzymes. Many details of the pathway, as well as the relative importance of these enzymatic forms in catalyzing starch degradation in developing endosperm, remain largely elusive.

DBE activity is necessary for proper starch biosynthesis. All plants characterized to date contain 2 conserved types of DBE: isoamylase-type DBE (ISA) and pullulanase-type DBE (PUL) (12). In maize, the complete set of DBEs consists of 1 *Zea mays* PUL1 (ZPU1) and 3 highly conserved ISA proteins (ISA1, ISA2, and ISA3). ISA1, encoded by *Sugary1* (*Su1*), is thought to be majorly responsible for amylopectin crystallinity and biosynthesis (13). Allelic mutations of *su1* elevate soluble sugars and a highly branched water-soluble polysaccharide (WSP), phytoglycogen, at

Significance

Maize *sugary enhancer1* (*se1*) is a genetic modifier of *su1* expression and is a commercially important allele that modifies kernel carbohydrate metabolism and improves fresh market quality. Carbohydrates, and primarily starch, are a major globally important product of cereal grains, but mechanisms affecting grain composition and genetic networks are not fully understood. In this study, we identify a gene that affects endosperm carbohydrate composition by modifying metabolism in a *sugary1* background. This discovery provides another entry point to understand metabolism and genetic background effects in cereal grains.

Author contributions: X.Z., K.J.H.v.M., C.N.H., W.F.T., and S.M.K. designed research; X.Z., K.J.H.v.M., V.S.L., B.D.V., and H.F.K. performed research; X.Z., K.J.H.v.M., V.S.L., C.N.H., B.D.V., H.F.K., and S.M.K. analyzed data; and X.Z., K.J.H.v.M., V.S.L., C.N.H., H.F.K., and S.M.K. wrote the paper.

The authors declare no conflict of interest.

This article is a PNAS Direct Submission.

Data deposition: Sequence information reported in this paper has been deposited in the GenBank database, www.ncbi.nlm.nih.gov/genbank (accession nos. KR154229 [W822GSe] and KR296736 [W822Gse]). Raw sequence reads used for single-nucleotide polymorphism identification and transcriptome analysis are available through the National Center for Biotechnology Information Sequence Read Archive, http://www.ncbi.nlm.nih.gov/sra (BioProject PRJNA287265).

[1]X.Z., K.J.H.v.M., and V.S.L. contributed equally to this work.

[2]To whom correspondence may be addressed. Email: smkaeppl@wisc.edu.

This article contains supporting information online at www.pnas.org/lookup/suppl/doi:10.1073/pnas.1902747116/-/DCSupplemental.

First Published September 23, 2019.

the expense of amylopectin (9, 14). Loss of Su1 function also results in a concomitant deficiency in the activity of ZPU1 (15). Recessive *su1* mutations are the basis of traditional sweet corn varieties. The *su1-ref* allele, which harbors a single-nucleotide polymorphism (SNP) that converts tryptophan to arginine, has been extensively used in modern sweet corn improvement, together with other endosperm mutations (14, 16, 17).

sugary enhancer1 (*se1*), a previously uncharacterized mutant affecting starch synthesis, is a recessive modifier of *su1*. Sweet corn homozygous for *su1* and *se1* alleles accumulates soluble sugars in kernels at approximately twice the concentration of kernels homozygous for *su1* allele and wild-type *Se1* allele, while maintaining the characteristic creamy texture conferred by WSP that is unique to *su1* mutant kernels (18, 19). Elevated maltose levels have been observed in mature dry *se1* mutant kernels; however, this trait was not always indicative of *se1* locus in all genetic backgrounds (20–22). Previous studies have postulated the *se1* locus at different locations and chromosomes in the maize genome (23, 24) due to the difficulty of scoring the presence of *se1* in dry seeds, as well as the complex genetic background effects on phenotype. This disparity has hindered the identification of the *Se1* gene and determination of its function.

Although the *se1* allele has been successfully incorporated into many sweet corn varieties with improved fresh market quality, its molecular identity was not known. The goal of this study was to identify the causative variant and molecular genetic basis of *se1* in starch metabolism. We utilized a pair of near-isogenic lines (NILs), W822Gse and W822GSe, which Mendelize the *se1* locus in a homozygous *su1-ref* background. The kernel phenotype of *su1* maize is known to vary in different genetic backgrounds (25), and this particular background produced a relatively plump kernel phenotype, allowing segregating *se1* expression to manifest. Map-based cloning identified wild-type *Se1* as a gene, localized on chromosome 2, whose complete deletion causes the *se1* phenotype. Changed patterns of transcripts and metabolites suggest that the *se1* genetic lesion affects starch metabolism and results in sucrose and maltose accumulation. Transgenic RNA interference (RNAi)-mediated functional validation further confirmed the causal effect of *Se1* silencing on the wrinkled kernel phenotype and increased maltose content.

Results

W822Gse and W822GSe Have a Contrasting Kernel Phenotype and Carbohydrate Profile. Near isogenic lines homozygous for the *su1-ref* but segregating for the *se1* were developed from an initial cross between Wh8419 (*Su1/Su1 Se1/Se1 sh2/sh2*), a supersweet sweet corn inbred, and Terminator (*su1-ref/su1-ref Se1/se1 Sh2/Sh2*), a sweet corn hybrid heterozygous for *se1*. The F_1 progeny were self-pollinated, and a lineage initiated from an F_2 plant was bred by self-pollination for 8 additional generations, selecting in each generation for segregation of wrinkled and smooth kernel phenotypes on a self-pollinated ear. Following the eighth generation of true-breeding, smooth kernel (W822GSe [*su1-ref/su1-ref Se1/Se1 Sh2/Sh2*]) and wrinkled kernel (W822Gse [*su1-ref/su1-ref se1/se1 Sh2/Sh2*]) isolines were established. The *su1-ref* gene was cloned from W822GSe and verified by sequencing to be the *su1-ref* allele (*SI Appendix*, Fig. S1) (14, 16, 17). Since both isolines were determined to be homozygous for wild-type *Sh2* based on visual phenotype, it is not included further in the genotype descriptions of the materials.

The segregating ears in the mapping population showed a distinct kernel phenotype. The *se1* kernel homozygous for the mutant *se1* allele had a wrinkled and translucent phenotype while the *Se1* kernels (*Se1/Se1*, *Se1/se1*) showed a smooth and opaque phenotype (Fig. 1 *A* and *B*). The kernel phenotype was expressed uniformly across the ear in the W822Gse (*su1-ref/su1-ref se1/se1*) and W822GSe (*su1-ref/su1-ref Se1/Se1*) isolines (Fig. 1*C*). Mature kernels of W822Gse contained 29% more total sugar, 79% more WSP, and 47% less starch than W822GSe (Fig. 1*D* and *SI Appendix*, Table S1). Similar differences were observed with developing kernels at 22 d after pollination (DAP) (Fig. 1*E*). At this stage, W822Gse relative to W822GSe contained more WSP and less starch; however, no significant difference in the total sugar content between W822GSe and W822Gse was observed for immature kernels at this developmental stage (Fig. 1*E*).

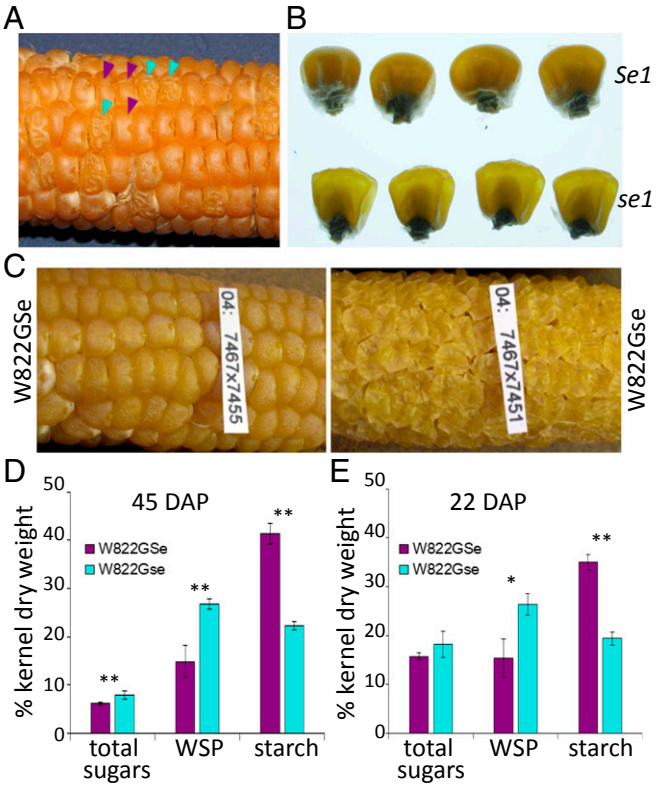

Fig. 1. *Se1* and *se1* phenotypes in the mapping population and near isogenic lines and their carbohydrate analysis. (*A*) Ear derived from self-pollination of a W822GSe x W822Gse cross segregating smooth *Se1* (homozygous [*Se1/Se1/Se1*] and heterozygous [*Se1/Se1/se1* and *Se1/se1/se1*], expressed as the genotype of the triploid endosperm) and wrinkled *se1* (homozygous [*se1/se1/se1*]) dry kernels. The purple and turquoise arrowheads indicate smooth and wrinkled kernels, respectively. (*B*) Individual smooth and wrinkled kernels viewed on a lightbox showing opaque and translucent phenotype, respectively. (*C*) W822GSe and W822Gse isolines homozygous for *Se1* and *se1* have uniformly smooth and wrinkled kernel phenotype, respectively. (*D* and *E*) Carbohydrate analysis of mature kernels at 45 d after pollination (DAP) (*D*) and immature kernels at 22 DAP (*E*) from W822GSe and W822Gse isolines. Frozen and lyophilized whole kernels from 3 ears of each genotype were analyzed for total sugar, water soluble polysaccharide (WSP), and starch content. Error bars are SD (SD, $n = 3$). *$0.01 < P < 0.05$; **$P < 0.01$. *Se1* and *se1* genotypes analyzed above are in the *su1-ref/su1-ref* genetic background.

We further evaluated starch accumulation in leaf tissue over the course of the 24-h light–dark cycle (*SI Appendix*, Fig. S2). A diurnal pattern of starch accumulation was observed beginning at dawn, with a decline in leaf carbohydrates beginning at dusk, but no significant differences were observed between W822Gse and W822GSe, indicating no effects of *se1* mutation on leaf starch content in the *su1-ref* background.

Map-Based Cloning Identified *Se1* as a Gene Localized at Chromosome 2. A total of 121 simple sequence repeat (SSR) markers throughout the maize genome (*SI Appendix*, Table S2) were used to comparatively examine W822Gse and W822GSe isolines. These markers were not a priori known to be informative in these lines so presence of polymorphism indicated a candidate region, but absence of polymorphism provided an ambiguous

PLANT BIOLOGY

result. A single marker, UMC1736, lying on the distal end of the long arm of chromosome 2, was found to be polymorphic and subsequently determined to be genetically linked to the wrinkled kernel trait, supporting this region as the location of *Se1*. The low marker diversity throughout the genome was consistent with a small introgression region. Subsequently, the boundaries of this region, as well as the isogenicity of the isolines, were further supported by genome-wide single nucleotide polymorphisms (SNPs) called from RNA sequencing (RNA-seq) data. The SNPs identified a region between 229,570,001 and 230,890,000 on chromosome 2 (AGPv2) as the introgression region.

Genetic mapping was initiated by crossing W822GSe and W822Gse to produce an F_1 hybrid that was self-pollinated to produce the segregating F_2 kernels. A ratio of 3:1 smooth:wrinkled kernels was observed on the progeny ears of self-pollinated F_1 individuals, supporting the hypothesis that the sugary enhancer trait is fully recessive and segregates as a single major gene. High-resolution mapping was conducted using UMC1736 and a flanking marker *Agt1*, which is proximal to *Se1* and UMC1736. The physical interval between *Agt1* and UMC1736 based on the B73 v2 reference genome assembly was 1.26 mega base pairs (Mbp) in length (Fig. 2*A*). The UMC1736 and *Agt1* markers were used to screen a population of 820 F_2 seedlings (representing 1,640 gametes) grown from phenotypically homozygous *se1*-type kernels selected from ears of self-pollinated F_1 plants. From these 1,640 gametes, 63 recombinants were identified between these 2 markers based on presence of the *Se1* parental allele at UMC1736, *Agt1*, or both. These DNA samples were systematically evaluated with 15 additional markers to increase the mapping resolution (*SI Appendix*, Table S3). This process narrowed *Se1* to an interval containing a single gene model, AC217415.3_FG004 (corresponding to Zm00001d007657 in gene model set Zm00001d.2) (Fig. 2 *B* and *C*). Three individuals remained heterozygous with the *Se1/se1* genotype for all markers throughout the region and were excluded as they likely resulted from hetero-fertilization events (26).

A 24.3-kb region encompassing *Se1* and the nearest proximal and distal gene models was sequenced in W822GSe and W822Gse. A notable variant observed in this sequence was a 637-bp deletion in the *se1* genotype, which completely eliminated the predicted coding sequence for Zm00001d007657 (Fig. 2*D*). A PCR marker developed for this deletion mutation perfectly cosegregated with the *se1* phenotype. Sequence data from the 6 closest cross-over events resulting from this group revealed that the cross-over events closest to the mutation occurred between SNPs at 297 and 170 bp from its proximal border, and between SNPs 197 and 39 bp from the distal border of the deletion. This supported that the deletion is the causal basis of the *se1* allele.

Putative Structure and Expression of the Wild-Type *Se1* Gene. Gene model Zm00001d007657 in B73 encodes a predicted protein comprising 173 amino acids of molecular weight 17.4 kDa, which would be translated from a GC-rich 522 bp sequence. Based on the gene model and expressed sequence tags (ESTs) available at https://www.maizegdb.org (EST GI: 31359437, 78025295, 5456061, and 5439303), *Se1* in B73 consists of only 1 exon with no introns. The *Se1* allele in W822GSe differs from the B73 reference allele with 11 SNPs, 2 in-frame insertions (3 and 6 nucleotides), and 2 insertions that cause a frameshift near the 3′ end (1 and 4 nucleotides), extending the length of the open reading frame (ORF) to 555 nucleotides and 184 amino acid residues.

Homology analysis of *Se1* revealed several homologous genes in monocots, including sorghum (*Sorghum bicolor*), grass species (*Aegilops tauschii*, *Panicum hallii*), rice (*Oryza sativa*), foxtail millet (*Setaria italica*), wheat (*Triticum aestivum*), and brachypodium (*Brachypodium distachyon*), but no orthologs were found in dicots. None of these orthologs have functional annotation available. In maize, the predicted SE1 protein contains a predicted conserved

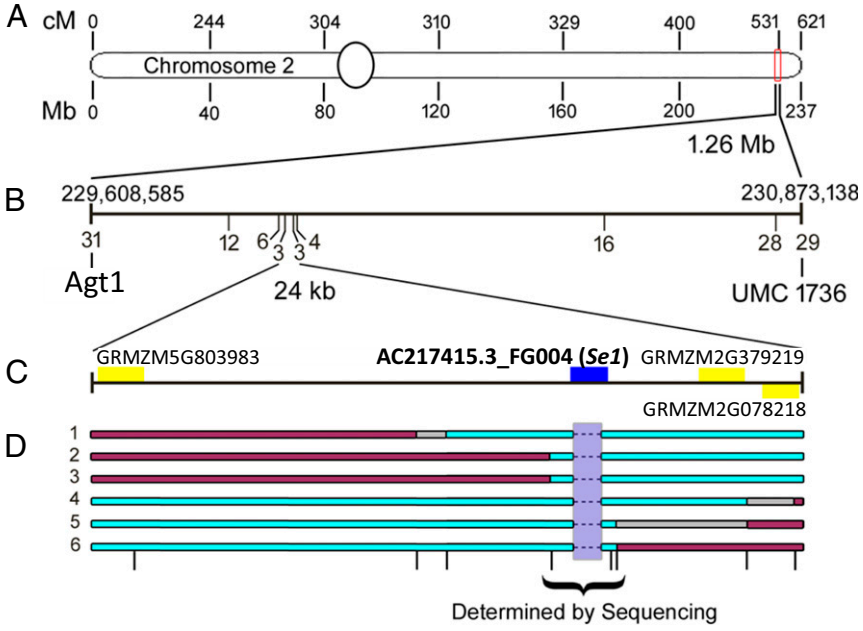

Fig. 2. Genetic mapping of *Se1*. (*A*) Location of *Se1* region on chromosome 2 indicated by the red box near the distal end. (*B*) Locus zoom of the *Se1* region in B73 showing the 1.26 Mb between the markers *Agt1* and UMC1736. Mapping markers and the number of recombinant plants with the *Se1* genotype from the mapping population are indicated by the vertical lines and associated numbers. (*C*) Locus zoom of the 24-kb region surrounding *Se1* in B73, with gene models indicated by the blue and yellow bars. AC217415.3_FG004 (*Se1*) is renamed Zm00001d007657 in gene model set Zm00001d.2 for assembly version Zm-B73-REFERENCE-GRAMENE-4.0. (*D*) Mapping data from 3 proximal and 3 distal recombinants (identified on the left). Vertical lines indicate marker locations. The purple bar represents regions *Se1/se1* genotypes, teal indicates *se1/se1* genotype, and gray indicates unknown genotype between markers. The genotypes of recombinants at the *Se1* locus were determined by sequencing. All recombinants shown and homozygous *se1/se1* controls possessed the deletion indicated by the light blue box and dotted lines, and all other gene models were excluded by the markers used for fine mapping.

FANTASTIC FOUR (FAF) domain. Proteins in this class have been shown to regulate shoot meristem size in *Arabidopsis* (27). Since regulation of meristem size is unlikely to be the basis of the modified endosperm biochemistry, SE1 can be characterized as a monocot-specific protein with unidentified function.

The spatiotemporal expression of *Se1* in B73 was examined by semiquantitative RT-PCR. The *Se1* transcript accumulated highly in the whole kernel, developing endosperm and leaf, but lowly in root and other tissues examined (*SI Appendix*, Fig. S3*A*). Dynamic *Se1* expression peaked in developing kernels at 16 to 20 DAP. *Se1* expression was also queried in the RNA-seq data published by Chen et al. (28) (*SI Appendix*, Fig. S3*B*) and expression profiles compiled in qTeller (*SI Appendix*, Fig. S3*C*). Consistently, *Se1* transcript was clearly detected in endosperm and embryo, with some differences for the developmental stage between different datasets, while RNA-seq profiles failed to detect *Se1* expression in any other tissues except leaf. The endosperm-predominant expression of *Se1* implies its spatial interaction in vivo with *Su1* since *Su1* is also expressed in the endosperm.

Comparative Metabolomic Analysis Revealed Distinct Differences in Starch and Sucrose Metabolism between W822Gse and W822GSe. In an effort to understand the role of *Se1* in metabolism, we conducted an untargeted metabolomics experiment comparing mutant *se1* and wild-type *Se1* isolines and reference inbred B73 over a time course of development. Developing endosperms harvested at 11 DAP to 21 DAP at 2-d intervals were subjected to gas chromatography-mass spectrometry (GC-MS) and ultra-performance liquid chromatography-MS (UPLC-MS) for metabolic profiling. In the UPLC-MS–based principal component analysis (PCA), the metabolic profile of W822Gse largely resembled that of W822GSe, indicating that the *Se1* deletion may exert small, likely indirect, effects on lipid metabolism since the majority of compounds identified from UPLC-MS belong to lipid classes (*SI Appendix*, Fig. S4).

In the GC-MS analysis, we unequivocally quantified 65 annotated metabolites. The score plot of PCA on annotated metabolites revealed a clear discrimination between the W822Gse mutant isoline and the W822GSe control isoline. The first principal component (PC1) explained the greatest variance (42.8%) in the dataset, separating the samples across sampling days (Fig. 3*A*). The third component (PC3) accounted for 11.3% of the variance and separated the samples by genotypes. We performed a 2-way ANOVA for all 65 annotated metabolites to identify those significantly affected by both genotype and development ($P < 0.05$). Fifteen metabolites involved in carbohydrate metabolism displayed significant changes across both genotypes and developmental time (*SI Appendix*, Fig. S5 and Table S4). Heat maps of metabolites were generated to visualize the relative metabolite changes across the developmental stages within the major compound families, including sugars and sugar phosphates, amino acids, organic acids, nucleotides, amines, and others (Fig. 3*B* and *SI Appendix*, Fig. S6). The group of sugars and sugar phosphates consisted of mono-, di-, and trisaccharides (fructose, glucose, raffinose, maltose, sucrose) and sugar phosphates (glucose-6-P, fructose-6-P, and mannose-6-P). Among them, sucrose and maltose were the only 2 sugar-related signatures showing significant differences between genotype and developmental stage (Fig. 3*B* and *SI Appendix*, Table S4). Starting at 15 DAP, W822Gse accumulated more sucrose than W822GSe, which had a sucrose level comparable to the reference B73 (Fig. 3*C*). Another striking difference was observed for maltose. From 17 DAP through 21 DAP, maltose content was significantly higher in W822Gse than in W822GSe and B73 and increased rapidly at later developmental stages while the other lines showed either trace amounts (B73) or slow accumulation (W822GSe) (Fig. 3*D*). Elevated sucrose and maltose levels conditioned by *se1* mutation confirmed that the mutant was behaving as predicted, supporting the role of *se1* in starch metabolism.

Transcript Profiling Indicated That *Se1* Affects Starch Biosynthesis and Degradation Processes. To identify genes involved in starch metabolism, as well as developmental and biochemical pathways affected by the *se1* mutation, we performed transcriptional profiling on the developing endosperm of W822Gse and W822GSe collected at 11, 15, and 19 DAP. RNA-seq generated an average of 14 million 100-bp single-end reads for each sample. Approximately 70% of these short reads were uniquely mapped to the B73 reference genome assembly (*SI Appendix*, Table S5).

Genes differentially expressed between W822Gse and W822GSe were compared with respect to the developmental stages. In total, 481 and 1,542 differentially expressed genes (DEGs) were identified at 15 and 19 DAP, respectively; of these, 179 and 660 genes were down-regulated, and 292 and 872 genes were up-regulated in W822Gse, respectively (Fig. 4*A*). Far fewer DEGs were detected at 11 DAP, with 27 up-regulated and 22 down-regulated in W822Gse. Among all of the DEGs, 24 genes are commonly shared among all 3 stages, with 20 genes up-regulated and 4 down-regulated in W822Gse relative to W822GSe (Fig. 4*A*). Interestingly, endosperm development appeared to have a pronounced impact on the differential gene expression, as indicated by the increasing number of DEGs across development from 49 DEGs at 11 DAP to the 1,542 at 19 DAP. Furthermore, we used MapMan analysis to map the transcriptome profiles and display important metabolic pathways for genes differentially expressed in the 2 isolines at different stages of endosperm development. Transcriptional mapping revealed similar functional categories for DEGs at 11, 15, and 19 DAP mainly in carbohydrate (CHO) and amino acid metabolism (*SI Appendix*, Fig. S7). For instance, DEGs regulated at 15 DAP fell predominately into the starch and sucrose metabolic pathway. These results largely corroborate the metabolomic observations.

Gene ontology (GO) enrichment analysis was conducted on DEGs to further characterize overrepresented biological process and molecular function associated with the *se1*. No significantly enriched GO terms related to metabolic pathways were identified with genes up-regulated in W822Gse at 11 and 15 DAP. However, down-regulated genes in W822Gse at 11 and 15 DAP showed significant association with starch metabolism. Remarkably, genes down-regulated in W822Gse at 15 DAP were enriched for biological processes related to starch biosynthesis such as "starch biosynthetic process," "glucan biosynthetic process," and "amylopectin biosynthetic process" (Fig. 4*B* and Dataset S1). Many known starch biosynthetic genes exhibited decreased expression in W822Gse at 11 and/or 15 DAP, including those encoding starch synthase (*Wx1*, *Su2*), starch branching and debranching enzymes (*Ae1*, *Sbe1*, *Su1*), and subunit of AGPase (*Sh2*, *Bt2*), sucrose synthase (*Sh1*), and ADPGlc transporter (*Bt1*) (Fig. 4*C*). At 19 DAP, a few starch biosynthetic genes, such as *Ae1*, *Su1*, and 2 AGPase small subunits (*Agp1* and *Agp2*), were down-regulated in W822Gse although no GO terms were significantly enriched for the starch biosynthesis pathway (Fig. 4*C* and Dataset S1). Interestingly, hydrolase activity (GO: 0004553) was overrepresented for genes up-regulated in W822Gse at 19 DAP, with 22 genes coding for glycosyl hydrolase family enriched (Dataset S1). Among them, *Zpu1*, encoding a known pullulanase-type DBE capable of hydrolyzing α-(1→6)–glucosidic bonds contributing to starch degradation in amylopectin, exhibited enhanced expression in W822Gse at 19 DAP (Dataset S1). These results suggest that the absence of *Se1* may affect starch metabolism by promoting starch degradation and inhibiting starch synthesis, yielding sucrose and maltose as end products in the *Se1*-absent genotype W822Gse. Further analysis will be required to validate the speculations made from the GO term analysis.

RNAi-Mediated Inhibition of *Se1* and *Su1* Expression in Transgenic Maize Conditioned *Se1*-Associated Morphological and Metabolic Traits. To validate the function of the wild-type *Se1*, we generated RNAi transgenic maize lines targeting only *Se1* (*Se1*-RNAi),

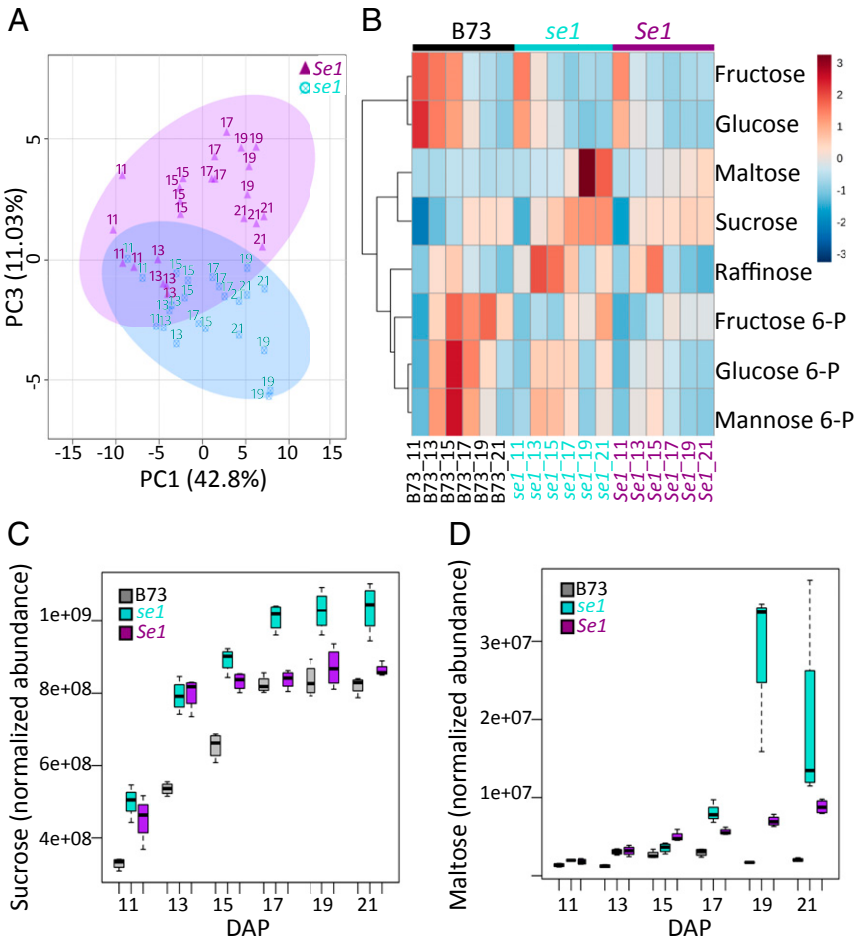

Fig. 3. Metabolic changes associated with mutant allele *se1*. (*A*) Scores plot from principal component analysis (PCA) of GC-MS–based metabolic profile in the developing endosperm of *Se1* and *se1*. PC1, principal component 1; PC3, principal component 3. Each point indicates a metabolite profile of a biological replicate (n = 4, except for *se1*-11) at each development stage (11 to 21 DAP at 2-d interval). (*B*) Heat map visualization of relative abundance of sugars and sugar phosphates in the developing endosperm of B73, *Se1*, and *se1* (11 to 21 DAP at 2-d interval). Metabolite abundance was log transformed and auto-scaled (mean-centered and divided by the SD of each variable) to form virtual colors as presented in the color key. (*C* and *D*) Sucrose and maltose levels in the developing endosperm of B73, *Se1*, and *se1*. The normalized spectrum abundance as described in *Materials and Methods* was used to indicate the metabolite level. *Se1* and *se1* represent W822GSe and W822Gse isolines, respectively, which are in the *su1-ref*/*su1-ref* genetic background.

only *Su1* (*Su1*-RNAi), and both *Se1* and *Su1* (*Se1Su1*-RNAi). Three independent events for *Se1Su1*-RNAi (referred to as *Se1Su1*-RNAi_1 to - _3), 3 independent events for *Su1*-RNAi (referred as *Su1*-RNAi_1 to - _3) and 2 independent events for *Se1*-RNAi (referred as *Se1*-RNAi_1 and *Se1*-RNAi_2) were chosen for study. Segregation for the transgene (visualized by red fluorescent protein [RFP] signal) and kernel phenotype (wrinkled due to *Su1* suppression) was evaluated on the progeny of 3 successive generations (*SI Appendix*, Figs. S8–S15 and Table S7). In *Se1Su1*-RNAi_1 and *Su1*-RNAi_2 BC_1 progeny ears, segregation of wrinkled and nonwrinkled kernels occurred at approximately a 1:1 ratio, and all of the wrinkled kernels were also RFP-positive (*SI Appendix*, Figs. S8 and S12 and Table S7). This segregation pattern was expected from the presence:absence of a hemizygous transgene locus. Interestingly, only segregation of RFP, and no obvious kernel phenotype, was observed on the kernels of BC_1 ears from the other 2 events (*Se1Su1*-RNAi_2, *Se1Su1*-RNAi_3, *Su1*-RNAi_1 and *Su1*-RNAi_3) (*SI Appendix*, Figs. S9–S11 and S13). As anticipated, only segregation of RFP was observed in the *Se1*-RNAi BC_1 progeny ears (*SI Appendix*, Figs. S14 and S15). In subsequent backcrosses with B73, the transgene segregated in a 1:1 ratio based on RFP signal, but the wrinkled kernel phenotype was not consistently seen. In *Se1Su1*-RNAi and *Su1*-RNAi BC_2-self (self-pollinated) progeny ears, we observed a 3:1 segregation ratio for RFP and non-RFP kernels, with one-third of RFP kernels being wrinkled (*SI Appendix*, Table S7). The segregating ear and RFP and/or wrinkled kernel phenotype for *Se1Su1*-RNAi_1 BC_2-self progeny are shown in Fig. 5 *A* and *B*. The observed segregation of RFP and wrinkled kernel phenotype implies that homozygosity for the RNAi allele was necessary to give a wrinkled kernel phenotype in the increasingly B73 background. In addition, RNAi-induced silencing of *Su1* alone was sufficient to generate the wrinkled kernel phenotype, as expected by suppression of *Su1*. Silencing of *Se1* alone did not produce a visible phenotype. The kernel phenotype of the *Se1Su1*-RNAi lines was not different from the *Su1*-RNAi lines, which is consistent with observations that the *se1* phenotype is not clearly observable in most genetic backgrounds containing *su1-ref*, with the special isolines used in this study being an exception.

We then used the semiquantitative RT-PCR to estimate the steady-state RNA level for *Se1* and *Su1* in self-pollinated BC_2 progeny kernels, as well as in reference samples (B73, W822GSe, and W822Gse). *Su1* was transcriptionally detectable in B73, W822GSe, and W822Gse as expected with *su1-ref* (14). *Su1* expression was lower in *Se1Su1*-RNAi and *Su1*-RNAi transgenic kernels in comparison to the segregating nontransgenic null kernels

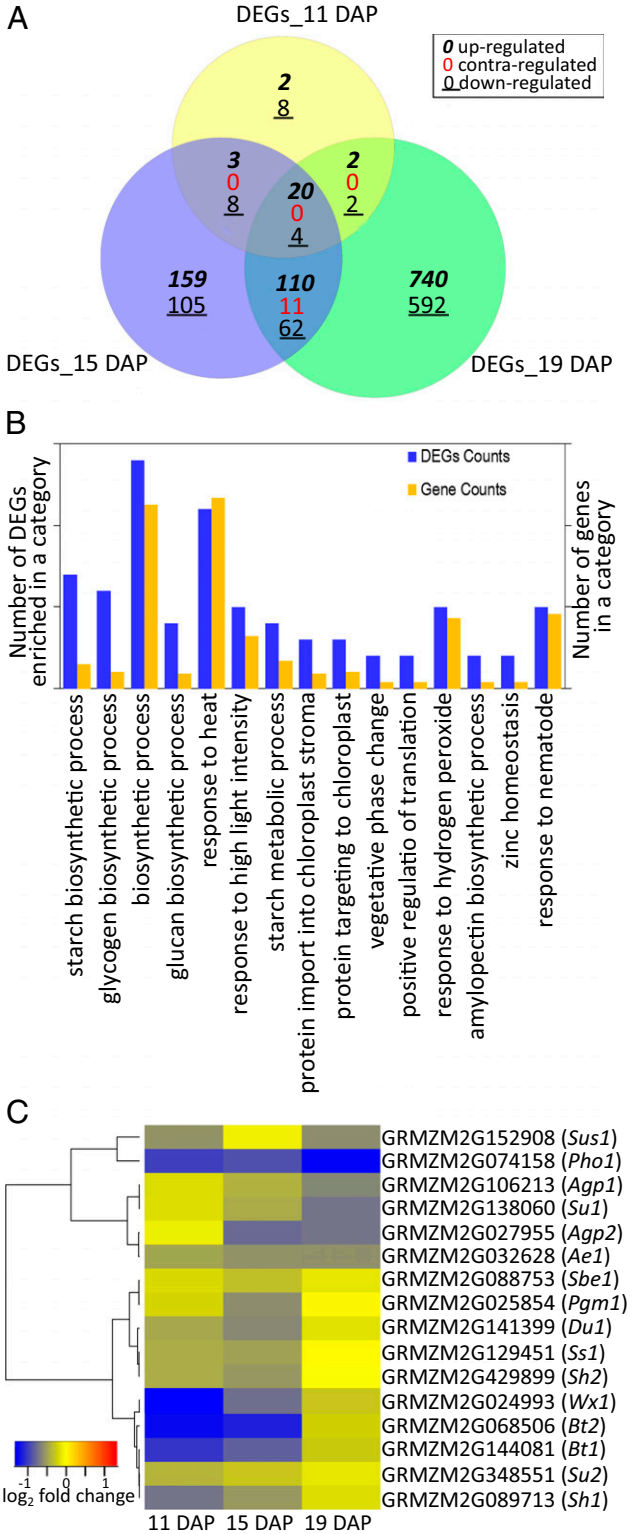

Fig. 4. Differentially expressed genes (DEGs) in W822Gse and W822GSe and enriched gene ontology (GO) terms for DEGs associated with starch metabolism. (*A*) Venn diagram of DEGs (FDR < 5%, |fold change| ≥ 1.5) between W822Gse and W822GSe at 11, 15, and 19 DAP. The number in each circle represents the amount of genes up-regulated (italic and bold), down-regulated (underlined), or contra-regulated (red) in W822Gse relative to W822GSe. (*B*) Significantly enriched GO categories associated with the down-regulated genes in W822Gse at 15 DAP. The left *y* axis indicates the number of DEGs enriched in a category; the right *y* axis shows the number of genes included in a category. (*C*) Heat map of DEGs involved in starch biosynthesis. Values of $\log_2$fold change (W822Gse vs. W822GSe) at 11, 15, and 19DAP were used for clustering.

and reference samples (Fig. 5*C*). *Se1* transcript showed normal accumulation in B73 and W822GSe but was absent in W822Gse. Decreased *Se1* expression was observed in *Se1Su1*-RNAi and *Se1*-RNAi transgenic kernels compared to segregating non-transgenic null kernels (Fig. 5*C*).

Our previous metabolomic profiling revealed that maltose was a distinct metabolic marker associated with *se1* mutation. We used this metabolic trait to validate the effect of reduced *Se1* in RNAi transgenic maize along with B73, W822GSe, and W822Gse reference samples. As anticipated, W822Se and W822se had significantly higher maltose than B73, with W822Gse having the highest maltose (Fig. 5*D*). For all of the 3 *Se1Su1*-RNAi and *Su1*-RNAi transgenic lines, transgenic kernels contained more maltose than sibling nontransgenic null kernels. No significant differences were observed in maltose content between *Se1*-RNAi transgenic kernels and sibling nontransgenic null kernels (Fig. 5*D*). Importantly, the average maltose content of transgenic kernels across the 3 *Se1Su1*-RNAi lines was significantly greater than the average maltose content of transgenic kernels across the 3 *Su1*-RNAi lines. These results indicate that reducing *Se1* expression in the presence of reduced *Su1* expression results in significantly increased maltose relative to reducing *Su1* expression alone, validating the causal role Zm00001d007657 as *Se1*.

Discussion

se1 is a widely used but previously uncharacterized endosperm mutation. In this study, we reported the cloning of the maize mutant *se1* and determined that the *se1* mutant phenotype is due to the absence of a putative gene, *Se1* (Zm00001d007657), located on chromosome 2. We comprehensively applied metabolic and transcriptional profiling to investigate its functional role in starch metabolism and employed the RNAi-mediated transgenic approach to functionally validate its causal role in producing the *se1* phenotype.

Using the high-resolution mapping population developed from a unique pair of isogenic lines contrasting for the sugary enhancer phenotype, we identified the *Se1* gene. Phenotypic segregation was 3:1 for smooth and wrinkled kernels in F_2 individuals, and an incremental increase in kernel sucrose and WSP was conditioned in plants homozygous for the *se1* allele (Fig. 1*A*). These observations unambiguously support *se1* as a single recessive locus responsible for the *se1* phenotype, and *se1* as modifier of *sugary1* since WSP is unique to the *su1* mutation. In agreement with genetic data, the predominant expression of *Se1* in the endosperm (*SI Appendix*, Fig. S3) similar to *Su1* and the exclusive differential carbohydrate profile in kernel rather than in leaf (Fig. 1 *D* and *E*) provide further substantial evidence supporting the causative basis of the sugary enhancer trait. Increased maltose levels were previously reported in sugary enhancer corn lines (20, 24). Our metabolic profiles conclusively identified the increase of sucrose and a concomitant accumulation of maltose in mutant W822Gse (Fig. 3). This result indicates that the elevated maltose level is more likely to be directly associated with *se1* allele as opposed to linked loci. Furthermore, RNAi-mediated inhibition of *Se1* and *Su1* expression in transgenic maize conferred the elevated maltose level and the wrinkled kernel phenotype (Fig. 5), 2 distinct morphological and metabolic traits that we characterized to be associated with the *se1* deletion in the *su1-ref* background, although the causal effect appears to be dependent on the genetic background.

The evidence obtained in this study, coupled with previous research, leads to several scenarios with regard to how *se1* may

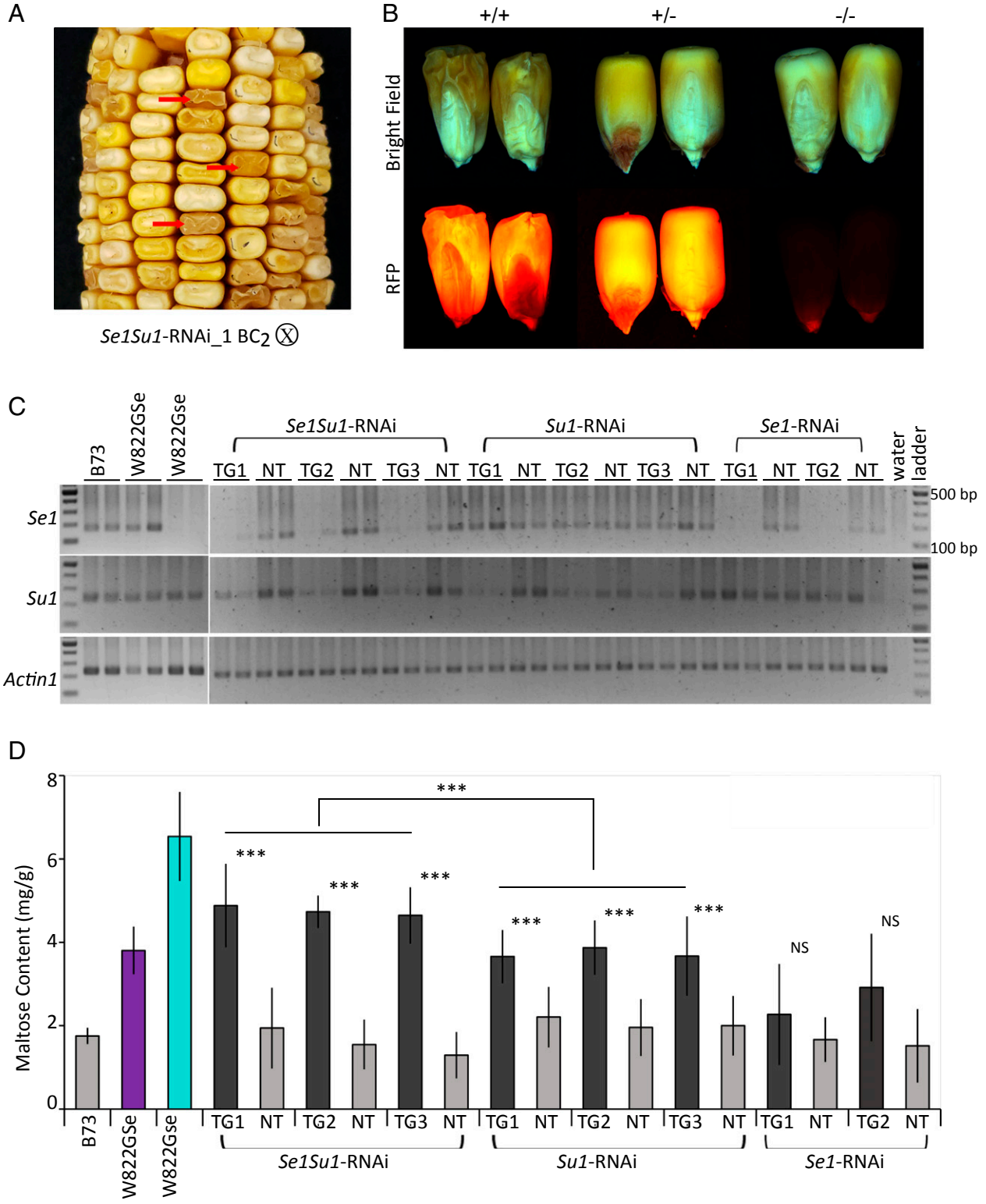

Fig. 5. Kernel traits and *Se1* and *Su1* expression in RNAi transgenic maize. (*A*) A representative ear of BC_2-self kernels on an ear from a self-pollinated *Se1Su1*-RNAi BC_2 progeny segregating for wrinkled kernels (red arrow). X represents self-pollinated. (*B*) Visualization of RFP and wrinkled kernel phenotype for individual kernels segregating in the ear shown in *A* using a Leica fluorescent dissecting microscope. +/+, RFP kernels exhibiting the wrinkled phenotype; +/–, kernels exhibiting only RFP signal; –/–, kernels showing no RFP or wrinkled kernel phenotype. (*C*) Analysis of *Se1* and *Su1* expression by semiquantitative RT-PCR in RNAi transgenic maize. Self-pollinated BC_2 progeny kernels of 3 independent events for *Se1Su1*-RNAi and *Su1*-RNAi and 2 events for *Se1*-RNAi (designated by TG1, TG2, and TG3) were used for analysis. B73, W822GSe, and W822Gse were used as references. TG and NT represent transgenic positive and nontransgenic sibling kernels. *Actin1* was used as an endogenous loading control. The expected amplicons of *Se1*, *Su1*, and *Actin* are 171, 234, and 230 bp, respectively. (*D*) Kernel maltose level in RNAi transgenic maize. Mean maltose content ($n = 14$) was determined in self-pollinated BC_2 progeny kernels (20 DAP) of 3 independent events for *Se1Su1*-RNAi and *Su1*-RNAi and 2 events for *Se1*-RNAi (designated by TG1, TG2, and TG3). B73, W822GSe, and W822Gse were used as references. TG and NT represent transgenic positive and nontransgenic sibling kernels. ***$P < 0.001$; NS, not significant (*t* test).

exert its effect in endosperm starch metabolism. Given the observations revealed by the joint metabolic and transcriptomic profiles that the *se1* deletion conditioned a unique pattern of maltose accumulation (Fig. 3), as well as enhanced transcript levels associated with hydrolase activity at later stages of endosperm development (Fig. 4), we would expect s*e1* to affect starch catabolism. Maltose is usually considered to be a major product of starch hydrolysis in nonliving endosperm cells of germinating cereal grain and starch mobilization in leaves (11, 29). In living endosperm cells, there will be no significant turnover of starch biosynthesis and degradation during the filling period when the rate of starch accumulation is close to that of starch synthesis (30). As previously reported in the endosperm of barley, some starch degradation occurs in parallel with starch synthesis during grain development (31). In maize mutant *se1*, high accumulation of sucrose at the expense of starch may interfere with the net starch accumulation and shift the transition to starch degradation, causing the elevated maltose levels particularly during late endosperm development. This corollary is supported by the enhanced expression of a group of genes encoding glycosyl hydrolases (GHs) in W822Gse at 19 DAP. Glycosyl hydrolases (GHs) comprise a superfamily of enzymes that cleave the glycosidic bonds in complex sugars and function in starch breakdown (32). With the exception of *Zpu1*, a pullulanase-type DBE that functions in starch degradation (15), the rest of the putative GH genes up-regulated in *se1* mutant are not present in the predicted starch degradation pathway of maize endosperm. There is a very limited list of annotated genes encoding major starch-degrading enzymes, consisting of α-amylases, β-amylases, limit dextran debranching enzymes, and α-glucosidase starch-degrading enzymes. Thus, we speculate that the contribution of *Se1* to starch degradation might be indirect; more likely, the wild-type *Se1* codes for a regulatory component inhibiting the expression of starch-degrading enzymes. Without this component in the *se1* mutant, starch hydrolysis is enhanced, and starch granules may become more susceptive to other enzymatic hydrolysis, generating glucan substrates for other degradation enzyme systems present in the endosperm and producing sucrose and maltose as end products.

The *se1* mutant phenotype includes increased WSP and decreased starch so the role of *se1* in developing maize endosperm cannot be solely via effects on starch degradation. Differential transcriptome analysis of these 2 isolines (W822GSe and W822Gse) revealed a concerted repression of essential starch biosynthetic genes in the *se1* mutant isoline (Fig. 4*B*), indicating that *se1* may enhance the *sugary1* phenotype by its pleiotropic effects on the expression of genes contributing to amylopectin biosynthesis. Mutations in starch biosynthesis genes commonly have pleiotropic effects on other starch biosynthesis enzymes in the same or different metabolic pathways (14, 33). A current explanation for widespread pleiotropic effects is that starch biosynthetic enzymes may operate as part of functional multiprotein complexes, which is evident from physical interactions among SS, SBE, and AGPase identified in both wheat and maize endosperm protein extracts (34–36). Such functional associations raise the possibility that *Se1* may act as a component of multisubunit complexes of starch biosynthetic enzymes. As such, the effects of the *Se1* deletion on starch metabolism could be attributable indirectly to altered activity of other starch biosynthetic enzymes. The possibility of *se1* having dual effects on both starch biosynthesis and starch degradation pathways is conceivable since there is a constant interplay between starch-synthesizing enzymes and starch-degrading enzymes (37). The inability to synthesize starch in *se1*, as well as the concomitant increase of free sucrose, may generate a metabolic imbalance, which could feed back and readjust metabolic pathways that fine tune the transition/turnover of starch biosynthesis and degradation. The subtle feedback-control mechanism makes sense in the context of the increased proportion of differentially expressed genes between the 2 isolines, which coincided with metabolic changes in sucrose and starch as the kernel development progressed.

Collectively, *se1* was identified here as a Mendelian factor affecting sucrose and starch content in maize endosperm. Our study represents a step forward in characterizing the gene nature and biological function of this commercially desirable *se1* allele. Beyond providing genotyping markers by which sweet corn breeders and researchers can more reliably discern the *se1* genotype, the *se1* allele may allow for the rapid introgression of this gene into elite maize backgrounds, thereby leading to greater commercial utilization. The findings bolster our knowledge of starch metabolism in cereal crops and provide another entry point to understand metabolism and genetic background effects in cereal grains. The remaining question about the precise localization of SE1 protein in starch metabolism and possible orchestrated relationships with other starch metabolic enzymes remain to be addressed in the future.

Materials and Methods

Genetic Stocks. Near isogenic lines (W822GSe and W822Gse) and derived progeny were utilized in the genetic mapping and subsequent metabolic and transcriptional analyses. Their origins are described in more detail in *Results*. RNA interference (RNAi) transgenic maize lines were generated as detailed in *Construct Design and the Development of Transgenic Maize* and *SI Appendix* and were used for analyzing kernel phenotype, *Se1* and *Su1* expression, and maltose content.

Carbohydrate Assay. Kernel and leaf carbohydrates, including total sugars, water-soluble polysaccharide (WSP), and starch, were determined in W822GSe and W822Gse isolines, as detailed in *SI Appendix*.

Genetic Analysis. RNA sequencing of the developing endosperm (11, 13, and 15 DAP) was used to identify genome-wide SNPs and validate the near isogenic nature of W822GSe and W833Gse. RNA isolation, library preparation, and sequencing strategy, as well as reads mapping and alignment, are in more detail described in *SI Appendix, Transcriptome Analysis*. Contrasting genotype scores between the isolines were determined based on RNA sequencing reads. Scores were only called at positions with at least 2 reads supporting a call and only homozygous calls were used in the analysis.

W822GSe and W822Gse kernels were germinated from 3 different ears to obtain biological replications for each genotype. DNA was isolated using the CTAB method (38), and all primers were designed with Primer 3 to flank introns based on the B73 reference sequence. Genome-wide SSR marker primers were obtained from https://www.maizegdb.org. Genes and gene fragments were identified based on expression evidence from ESTs, and/or by gene models in ORFs predicted by FGENESH. PCRs were performed with a touch-down protocol using HotStarTaq DNA polymerase (Qiagen) or AccuPrime GC-Rich DNA polymerase (Thermo Fisher Scientific). Successful amplifications were subject to Sanger sequencing and polymorphism analysis by BioEdit. F_2 mapping populations were screened for polymorphisms through direct sequencing, RFLP, and KASPar SNP assays. A 24.3-kb region flanking the candidate gene was assembled in BioEdit and deposited in GenBank under accession numbers KR154229 (W822GSe) and KR296736 (W822Gse).

To genotype the *Se1* gene at the site of the deletion, a 3-primer PCR approach was used, with details described in *SI Appendix*. To verify that the *su1* allele in W822Se is *su1-ref*, the *su1* allele was cloned and sequenced, as detailed in *SI Appendix*.

Homology Analysis of *Se1* and Its Spatial–Temporal Expression. The B73 sequence for Zm00001d007657 was used to perform BLASTN and TBLASTX searches against the nr/nt databases at the National Center for Biotechnology Information (NCBI) and Gramene. A conserved domain search service was performed to identify the conserved domains present in the SE1 protein sequence (39). All analyses above were performed with default parameters. RT-PCR was performed to analyze the spatial and temporal expression of *Se1* in B73 as detailed in *SI Appendix*.

Metabolome Analysis. Nontarget metabolite profiling was performed with developing endosperm (2-d intervals from 11 to 21 DAP) of B73 and 2 isolines at the Proteomics and Metabolomics Facility (Colorado State University). Sample preparation was based on the methyl tert-butyl ether (MTBE)/methanol/water extraction method (40), which allows the separation of the upper lipid-containing organic phase and the lower aqueous phase for

UPLC-MS and GC-MS analysis, respectively. Feature detection and alignment were performed using the open source XCMS package (41). Dataset-wide correlational grouping and compound annotation were performed using in-house tools by spectral matching to in-house NISTv12 (NIST/EPA/NIH Mass Spectral Library, National Institute of Standards and Technology), Golm, Metlin (https://metlin.scripps.edu), and Massbank metabolite databases (42–44). The peak areas for each feature in a spectrum were condensed via the weighted mean of all features in a spectrum into a single value for each compound. Analysis of variance was conducted on each compound using the aov function in R, and *P* values were adjusted for false positives using the Bonferroni–Hochberg method in the p.adjust function in R. Principal component analysis (PCA) and heat maps of metabolites were conducted on mean-centered and auto variance-scaled data using MetaboAnalyst 3.0 (45).

Transcriptome Analysis. Developing endosperm collected from 2 random W822GSe and W822Gse plants at 6 developmental stages (2-d intervals from 11 to 21 DAP) was used for transcriptome analysis. Details about RNA isolation, library construction, RNA-seq, and data analysis are provided in *SI Appendix*. Raw sequence reads are available through the National Center for Biotechnology Information Sequence Read Archive under BioProject PRJNA287265.

Differentially expressed genes (DEGs) were identified by pairwise comparisons using edgeR (46). Only genes with read counts >1 were used for differential expression analysis, and genes were considered differentially expressed if the false discovery rate (FDR) (*P* value after adjusting for false discovery rate) was ≤0.05 and the absolute value of the fold change was ≥1.5. A heat map with dendrograms was produced with the pheatmap R package (47). DEGs were assigned to metabolic pathways and subsequently visualized using Mapman software based on the functional annotation file ZmB73_5b_FGS_cds_2012 (https://mapman.gabipd.org/mapman) (48). Gene Ontology (GO) analysis of DEGs was performed with the goseq package in R using the Wallenius approximation method (49). GO term annotations for maize genes were obtained from Gramene (https://archive.gramene.org/plant_ontology/). All calculations and plotting were performed in R (version 3.4.2).

Construct Design and the Development of Transgenic Maize. We generated the RNA interference (RNAi)-mediated transgene(s) targeting only *Se1* (*Se1*-RNAi), only *Su1* (*Su1*-RNAi), and both *Se1* and *Su1* (*Se1Su1*-RNAi). A 368-bp *Se1* target region (bases 152 to 519 of *Se1* [Zm00001d007657]) and a 372-bp *Su1* target region (bases 643 to 1014 of *Su1* [Zm00001d049753]) and their fusion fragment were chemically synthesized and cloned in inverted repeats into the binary vector pANIC8D through Gateway cloning technology (50). The resulting dual-target RNAi vector contains the hairpin sequence driven by the maize ubiquitin 1 promoter and enhancer intron 1, the bialaphos resistance gene (*bar*) driven by the rice actin 1 promoter and intron 1 enhancer, and a red fluorescent protein (RFP) visual marker driven by the *Panicum virgatum* ubiquitin 1 promoter. Maize line HiII (AxB) was transformed with RNAi constructs via *Agrobacterium*-mediated transformation (51). The presence of transgene was tracked by testing for bialaphos resistance, visual RFP signal, and/or the wrinkled kernel phenotype. The development and growth of transgenic maize lines and kernel harvest are detailed in *SI Appendix*.

Expression of *Se1* and *Su1* in Transgenic Maize. RT-PCR was performed to analyze the mRNA abundance of *Se1* and *Su1* in 20-DAP kernels harvested from BC_2-self transgenic lines and control, as detailed in *SI Appendix*.

Maltose Assay in Transgenic Maize. Maltose was measured on the 20-DAP kernels of 3 independent transgenic events that were harvested from self-pollinated BC_2 ears using the Maltose/Sucrose/D-Glucose Assay Kit (catalogue no. K-MASUG; Megazyme). Maltose content in B73, W822GSe, and W822Gse kernels, as well as sibling nontransgenic (null) kernels, was also assayed as control.

ACKNOWLEDGMENTS. We acknowledge the support of a National Research Initiative grant from the US Department of Agriculture Cooperative State Research, Education and Extension Service (CSREES/NRI 2007-55301-18179) and the Wisconsin Alumni Research Foundation Accelerator Program. We thank Rajan Sekhon for help with expression analysis and Nick Santoro for leaf carbohydrate processing. We thank the University of Wisconsin Biotechnology Center DNA Sequencing Facility for providing RNA-seq services. Mass spectrometry was performed by the Proteomics and Metabolomics Facility (Colorado State University). Research materials were grown at the University of Wisconsin Agricultural Research Stations (ARSs), and we specifically acknowledge assistance of Tom Wright at the West Madison ARS and Lynn Hummel at the ARS greenhouses.

1. A. Bahaji *et al*., Starch biosynthesis, its regulation and biotechnological approaches to improve crop yields. *Biotechnol. Adv.* **32**, 87–106 (2014).
2. A. M. Smith, K. Denyer, C. Martin, The synthesis of the starch granule. *Annu. Rev. Plant Physiol. Plant Mol. Biol.* **48**, 67–87 (1997).
3. L. C. Hannah, Starch synthesis in the maize endosperm. *Maydica* **50**, 497–506 (2005).
4. D. K. Fisher, M. Gao, K. N. Kim, C. D. Boyer, M. J. Guiltinan, Allelic analysis of the maize amylose-extender locus suggests that independent genes encode starch-branching enzymes IIa and IIb. *Plant Physiol.* **110**, 611–619 (1996).
5. K. N. Kim, D. K. Fisher, M. Gao, M. J. Guiltinan, Molecular cloning and characterization of the amylose-extender gene encoding starch branching enzyme IIB in maize. *Plant Mol. Biol.* **38**, 945–956 (1998).
6. J. M. Bae, M. J. Giroux, L. C. Hannah, Cloning and characterization of the Brittle-2 gene of maize. *Maydica* **35**, 317–322 (1990).
7. P. S. Chourey, O. E. Nelson, The enzymatic deficiency conditioned by the shrunken-1 mutations in maize. *Biochem. Genet.* **14**, 1041–1055 (1976).
8. M. R. Bhave, S. Lawrence, C. Barton, L. C. Hannah, Identification and molecular characterization of shrunken-2 cDNA clones of maize. *Plant Cell* **2**, 581–588 (1990).
9. M. G. James, D. S. Robertson, A. M. Myers, Characterization of the maize gene sugary1, a determinant of starch composition in kernels. *Plant Cell* **7**, 417–429 (1995).
10. M. Shure, S. Wessler, N. Fedoroff, Molecular identification and isolation of the Waxy locus in maize. *Cell* **35**, 225–233 (1983).
11. A. M. Smith, S. C. Zeeman, S. M. Smith, Starch degradation. *Annu. Rev. Plant Biol.* **56**, 73–98 (2005).
12. M. K. Beatty *et al*., Purification and molecular genetic characterization of ZPU1, a pullulanase-type starch-debranching enzyme from maize. *Plant Physiol.* **119**, 255–266 (1999).
13. A. Kubo *et al*., Functions of heteromeric and homomeric isoamylase-type starch-debranching enzymes in developing maize endosperm. *Plant Physiol.* **153**, 956–969 (2010).
14. J. R. Dinges, C. Colleoni, A. M. Myers, M. G. James, Molecular structure of three mutations at the maize sugary1 locus and their allele-specific phenotypic effects. *Plant Physiol.* **125**, 1406–1418 (2001).
15. J. R. Dinges, C. Colleoni, M. G. James, A. M. Myers, Mutational analysis of the pullulanase-type debranching enzyme of maize indicates multiple functions in starch metabolism. *Plant Cell* **15**, 666–680 (2003).
16. W. F. Tracy, S. R. Whitt, E. S. Buckler, Recurrent mutation and genome evolution: Example of sugary1 and the origin of sweet maize. *Crop Sci.* **46** (suppl. 1), S49–S54 (2006).
17. B. D. De Vries, W. F. Tracy, Characterization of endosperm carbohydrates in isa2–339 maize and interactions with su1-ref. *Crop Sci.* **56**, 2277–2286 (2016).
18. J. W. Gonzales, A. M. Rhodes, D. B. Dickinson, A new inbred with high sugar content in sweet corn. *HortScience* **9**, 79–80 (1974).
19. J. W. Gonzales, A. M. Rhodes, D. B. Dickinson, Carbohydrate and enzymic characterization of a high sucrose sugary inbred line of sweet corn. *Plant Physiol.* **58**, 28–32 (1976).
20. J. E. Ferguson, D. B. Dickinson, A. M. Rhodes, Analysis of endosperm sugars in a sweet corn inbred (Illinois 677a) which contains the sugary enhancer (se) gene and comparison of se with other corn genotypes. *Plant Physiol.* **63**, 416–420 (1979).
21. E. E. Carey, A. M. Rhodes, D. B. Dickinson, Post-harvest levels of sugars and sorbitol in sugary enhancer (su se) and sugary (su Se) maize. *HortScience* **17**, 241–242 (1982).
22. D. R. L. Bonte, J. A. Juvik, Characterization of sugary1 (su1) sugary enhancer (se) kernels in segregating sweet corn populations. *J. Am. Soc. Hortic. Sci.* **155**, 153–157 (1990).
23. D. R. L. Bonte, J. A. Juvik, Sugary enhancer (se) gene located on the long arm of chromosome 4 in maize (*Zea mays L.*). *J. Hered.* **82**, 176–178 (1991).
24. Y. Tadmor, F. Azanza, T. Han, T. R. Rocheford, J. A. Juvik, RFLP mapping of the sugary enhancer1 gene in maize. *Theor. Appl. Genet.* **91**, 489–494 (1995).
25. B. D. De Vries, S. L. Shuler, W. F. Tracy, Endosperm carbohydrates in pseudostarchy and extreme-sugary maize inbreds during kernel development. *Crop Sci.* **56**, 2448–2456 (2016).
26. G. F. Sprague, The nature and extent of hetero-fertilization in maize. *Genetics* **17**, 358–368 (1932).
27. V. Wahl, L. H. Brand, Y.-L. Guo, M. Schmid, The FANTASTIC FOUR proteins influence shoot meristem size in Arabidopsis thaliana. *BMC Plant Biol.* **10**, 285 (2010).
28. J. Chen *et al*., Dynamic transcriptome landscape of maize embryo and endosperm development. *Plant Physiol.* **166**, 252–264 (2014).
29. A. M. Smith, S. C. Zeeman, D. Thorneycroft, S. M. Smith, Starch mobilization in leaves. *J. Exp. Bot.* **54**, 577–583 (2003).
30. K. Tomlinson, K. Denyer, "Starch synthesis in cereal grains" in *Advances in Botanical Research*, J. A. Callow, Ed. (Academic Press, 2003), vol. **40**, pp. 1–61.
31. V. V. Radchuk *et al*., Spatiotemporal profiling of starch biosynthesis and degradation in the developing barley grain. *Plant Physiol.* **150**, 190–204 (2009).
32. L. Tyler *et al*., Annotation and comparative analysis of the glycoside hydrolase genes in Brachypodium distachyon. *BMC Genomics* **11**, 600 (2010).
33. M. J. Giroux, C. Boyer, G. Feix, L. C. Hannah, Coordinated transcriptional regulation of storage product genes in the maize endosperm. *Plant Physiol.* **106**, 713–722 (1994).
34. I. J. Tetlow *et al*., Analysis of protein complexes in wheat amyloplasts reveals functional interactions among starch biosynthetic enzymes. *Plant Physiol.* **146**, 1878–1891 (2008).
35. T. A. Hennen-Bierwagen *et al*., Proteins from multiple metabolic pathways associate with starch biosynthetic enzymes in high molecular weight complexes: A model for regulation of carbon allocation in maize amyloplasts. *Plant Physiol.* **149**, 1541–1559 (2009).
36. Z. Ahmed, I. J. Tetlow, R. Ahmed, M. K. Morell, M. J. Emes, Protein-protein interactions among enzymes of starch biosynthesis in high-amylose barley genotypes reveal differential roles of heteromeric enzyme complexes in the synthesis of A and B granules. *Plant Sci.* **233**, 95–106 (2015).

37. A. Whan *et al*., Engineering α-amylase levels in wheat grain suggests a highly sophisticated level of carbohydrate regulation during development. *J. Exp. Bot.* **65**, 5443–5457 (2014).
38. J. Doyle, J. L. Doyle, Isolation of plant DNA from fresh tissue. *Focus* **12**, 13–15 (1990).
39. A. Marchler-Bauer *et al*., CDD/SPARCLE: Functional classification of proteins via subfamily domain architectures. *Nucleic Acids Res.* **45**, D200–D203 (2017).
40. V. Matyash, G. Liebisch, T. V. Kurzchalia, A. Shevchenko, D. Schwudke, Lipid extraction by methyl-tert-butyl ether for high-throughput lipidomics. *J. Lipid Res.* **49**, 1137–1146 (2008).
41. C. A. Smith, E. J. Want, G. O'Maille, R. Abagyan, G. Siuzdak, XCMS: Processing mass spectrometry data for metabolite profiling using nonlinear peak alignment, matching, and identification. *Anal. Chem.* **78**, 779–787 (2006).
42. J. Kopka *et al*., GMD@CSB.DB:The Golm metabolome database. *Bioinformatics* **21**, 1635–1638 (2005).
43. H. Horai *et al*., MassBank: A public repository for sharing mass spectral data for life sciences. *J. Mass Spectrom.* **45**, 703–714 (2010).
44. C. D. Broeckling, A. L. Heuberger, J. A. Prince, E. Ingelsson, J. E. Prenni, Assigning precursor–Product ion relationships in indiscriminant MS/MS data from non-targeted metabolite profiling studies. *Metabolomics* **9**, 33–43 (2013).
45. J. Xia, I. V. Sinelnikov, B. Han, D. S. Wishart, MetaboAnalyst 3.0—Making metabolomics more meaningful. *Nucleic Acids Res.* **43**, W251–W257 (2015).
46. M. D. Robinson, D. J. McCarthy, G. K. Smyth, EdgeR: A Bioconductor package for differential expression analysis of digital gene expression data. *Bioinformatics* **26**, 139–140 (2010).
47. R. Kolde, pheatmap: Pretty Heatmaps. R package Version 0.7.7. https://cran.r-project.org/web/packages/pheatmap/index.html. Accessed 4 January 2019.
48. O. Thimm *et al*., MAPMAN: A user-driven tool to display genomics data sets onto diagrams of metabolic pathways and other biological processes. *Plant J.* **37**, 914–939 (2004).
49. M. D. Young, M. J. Wakefield, G. K. Smyth, A. Oshlack, Gene ontology analysis for RNA-seq: Accounting for selection bias. *Genome Biol.* **11**, R14 (2010).
50. D. G. J. Mann *et al*., Gateway-compatible vectors for high-throughput gene functional analysis in switchgrass (Panicum virgatum L.) and other monocot species. *Plant Biotechnol. J.* **10**, 226–236 (2012).
51. B. Frame, M. Main, R. Schick, K. Wang, "Genetic transformation using maize immature zygotic embryos" in *Plant Embryo Culture: Methods and Protocols*, T. A. Thorpe, E. C. Yeung, Eds. (Humana Press, Totowa, NJ, 2011), pp. 327–341.